Electronic Supplementary Material (ESI) for Journal of Materials Chemistry A.
This journal is © The Royal Society of Chemistry 2016

Supplementary Information

Ultrafast laser-assisted synthesis of hydrogenated molybenum oxides for flexible organic solar cells

*Wan Jae Dong, Juyoung Ham, Gwan Ho Jung, Jun Ho Son and Jong-Lam Lee**

Surface morphology and sheet resistance of ITO/MoO_3

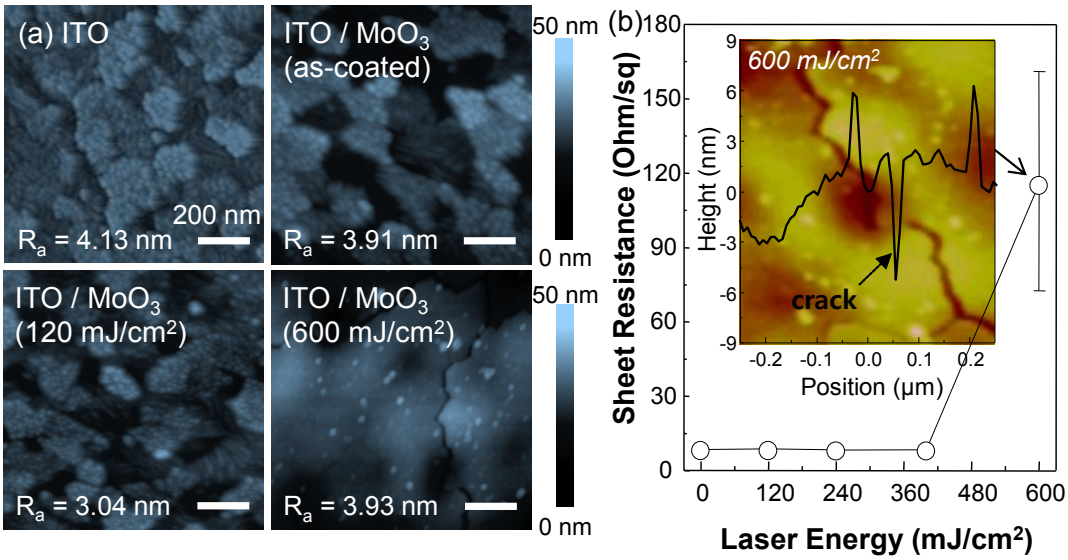

Figure S1. (a) Atomic force microscopy images of ITO electrode, as-coated MoO_3 and treated MoO_3 with laser energy of 120 mJ/cm^2 and 600 mJ/cm^2. Scale bar: 200 nm. (b) Measured sheet resistance of ITO/MoO_3. Inset: height profile of AFM topography of ITO/MoO_3 after 600 mJ/cm^2 laser irradiation.

The surface morphology of ITO electrode, as-coated MoO_3 layer and laser-irradiated MoO_3 layers are indicated in Figure S1a. The ITO electrode has average roughness (R_a) of 4.13 nm. This roughness comes from the grain and grain boundary of poly-crystalline ITO layer. After coating the MoO_3 solution on ITO electrode, the R_a is slightly decreased to 3.91 nm. But, the grain structure of ITO is still remained on the surface of MoO_3 layer. We believe that the MoO_3 precursors stacked on the grains and filled the voids between ITO grains, thereby resulting in decreased roughness. The laser irradiation with moderate energy of 120

mJ/cm^2 further decreases the R_a to 3.04 nm. The photons with the largest energy flux (600 mJ/cm^2) recrystallize the ITO layer, thereby resulting in large grain, crack formation and increased Ra (3.93 nm). All the samples show the similar averaged roughness (3.04 ~ 3.93 nm). However, when the high energy of 600 mJ/cm^2 is irradiated on the substrate, The cracks are formed in ITO layer due to thermal shock during recrystallization. These cracks significantly increase the average sheet resistance from 8 Ω/sq to 120 Ω/sq (Figure S1b).

Optical properties of H_yMoO_{3-x}

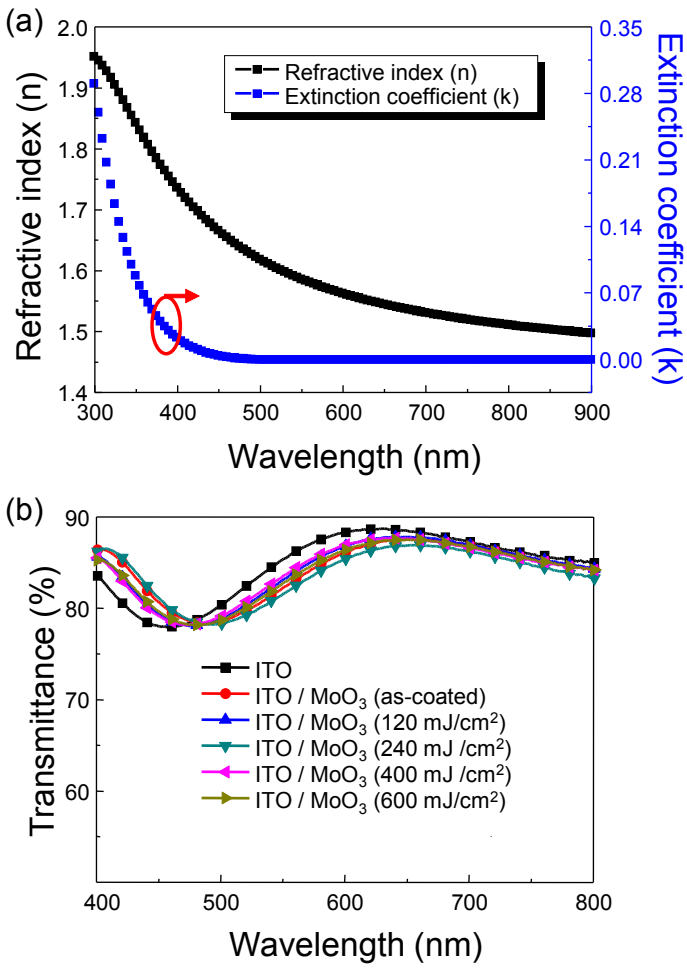

Figure S2. (a) Refractive index (n) and extinction coefficient (k) of H_yMoO_{3-x} measured by using optical ellipsometer. (b) Measured optical transmittance of glass/ITO/H_yMoO_{3-x} transparent electrodes.

Refractive index (n) and extinction coefficient of H_yMoO_{3-x} is plotted as a function of wavelength (Figure S2a). As the wavelength is increase from 300 nm to 900 nm, the refractive index is gradually decreases from 1.95 to 1.50. The extinction coefficient of H_yMoO_{3-x} rapidly decreases from 0.28 to 0.02 on the short wavelength region (λ = 300 ~ 400 nm). But, the extinction coefficient converges to zero when the wavelength exceeds 400 nm. This results confirms that the H_yMoO_{3-x} has bandgap energy of 3.3 ~ 3.4 eV. The optical transmittance of glass/ITO/MoO_3 structure are measured for various laser energies (Figure S2b). The average transmittance of ITO-coated glass substrate shows 84.6% (λ = 400 ~ 800 nm). The transmittance of MoO_3 exhibits 84.1% which doesn't change by laser irradiation.

Reaction time of laser-irradiation and thermal annealing

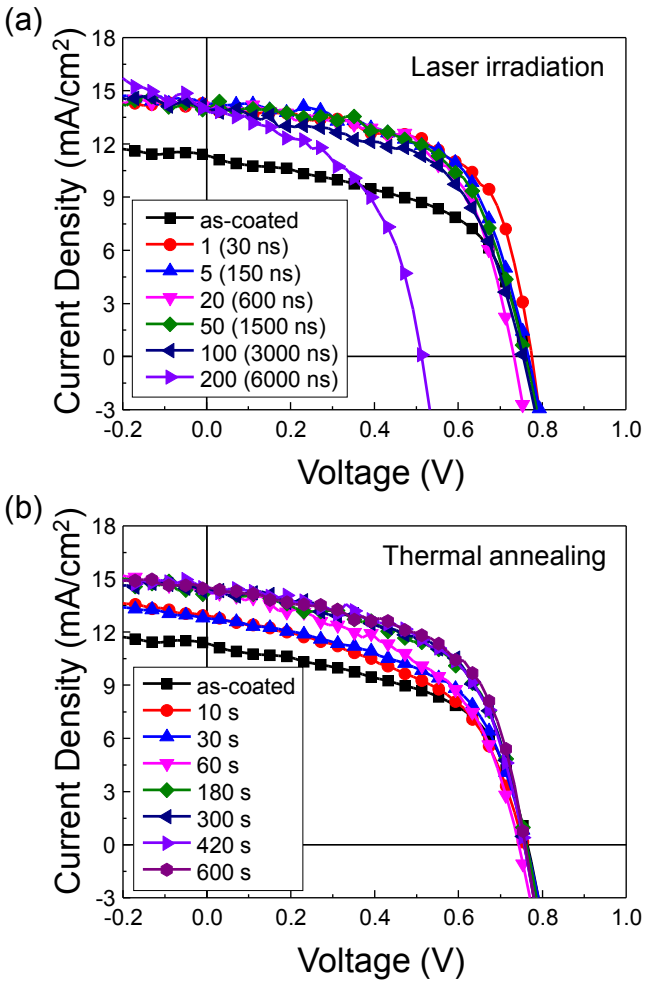

Figure S3. J-V characteristics of devices with MoO_3 by (a) laser irradiation (240 mJ/cm^2) and (b) thermal annealing at 150 ℃.

MoO_3 layers were demonstrated as hole transport layers in PTB7:PCBM OSCs. The laser energies (Figure S3a) and duration of thermal annealing (Figure S3b) were varied in order to compare the reaction time. The device with as-coated MoO_3 exhibits low photo-conversion efficiency of 4.7%, but it increases to 6.6% after irradiating one pulse (30 ns) of laser (240 mJ/cm^2). As increasing the number of laser irradiation, the device efficiency gradually decreased. On the other hand, the thermal annealed sample slowly increased PCE value. It requires more than 180s to achieve the efficiency higher than 6.0%. The highest efficiency was 6.3% which is slightly lower than device treated by laser-irradiation.

Table S1. A summary of the device performances obtained for PTB7:PCBM OSCs.

# of irradiation (exposure time)	**V_{oc} (V)**	**J_{sc} (mA/cm^2)**	**FF (%)**	**PCE (%)**
as-coated	0.77	11.4	53.0	4.7
1 (30 ns)	0.77	14.3	59.8	6.6
5 (150 ns)	0.77	14.2	59.1	6.5
20 (600 ns)	0.73	14.1	59.3	6.1
50 (1500 ns)	0.75	13.9	59.6	6.2
100 (3000 ns)	0.75	14.2	55.8	5.9
200 (6000 ns)	0.51	14.0	49.4	3.5
Thermal annealing time	**V_{oc} (V)**	**J_{sc} (mA/cm^2)**	**FF (%)**	**PCE (%)**
10 sec	0.75	12.9	49.8	4.8
30 sec	0.75	12.8	54.5	5.2
60 sec	0.73	14.2	51.1	5.3
180 sec	0.75	14.1	57.2	6.1
300 sec	0.75	14.3	57.9	6.2
420 sec	0.75	14.5	56.3	6.1
600 sec	0.75	14.5	58.3	6.3

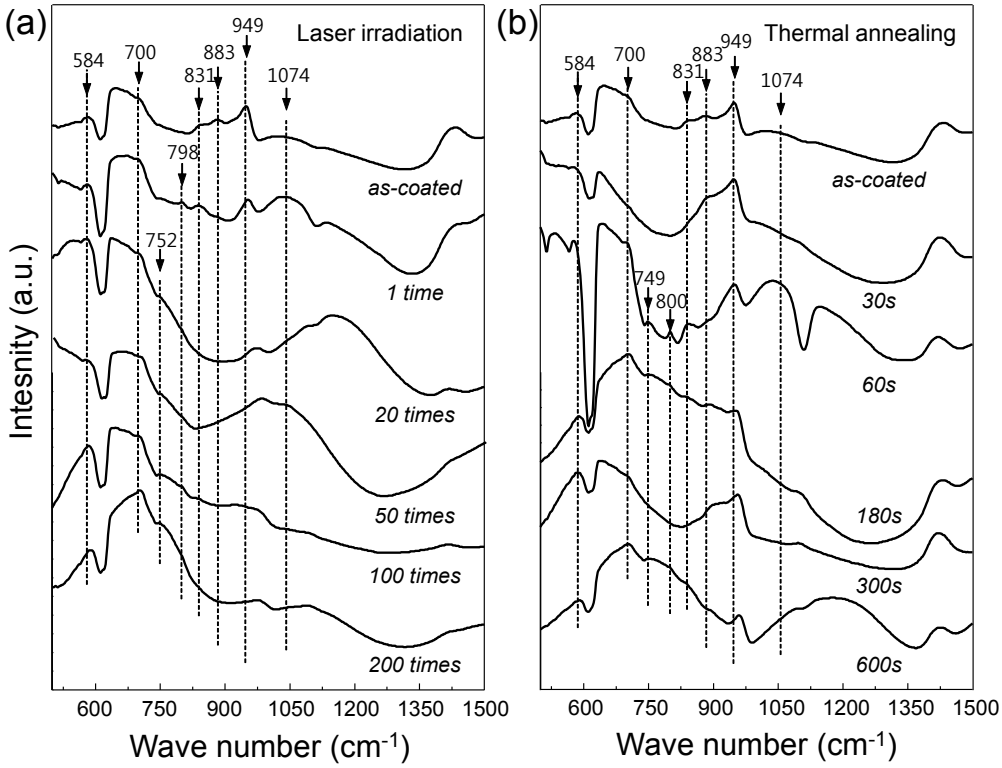

Figure S4. FTIR absorbance spectra of as-coated, laser-irradiated, and thermal annealed MoO_3.

The FTIR absorbance spectra of MoO_3 were measured for various number of laser irradiation (Figure S4a) and duration of thermal annealing (Figure S4b). As number of laser irradiation increases to 50 times, the vibration of terminal oxygen (O=Mo) at 949 cm^{-1} and the vibration of Mo-O-Mo (831 and 883 cm^{-1}) diminishes, but the broad Mo-O-H band (1050-1350 cm^{-1}) appears. When the number of laser irradiation exceeds 100 times, the absorption band of Mo-O-H vanished, meaning that the highly reduced state of Mo (Mo^{4+}) is largely produced in the MoO_3 layer. On the other hand, the thermal annealed samples show any noticeable change. The vibration of terminal oxygen (O=Mo) and Mo-O-Mo vibrations were remained even after the long thermal annealing of 600 s. We believe that low temperature thermal annealing (150 ˚C) cannot supply the activation energy for deboning the Mo-O bonds.

Internal quantum efficiency of PTB7:PCBM

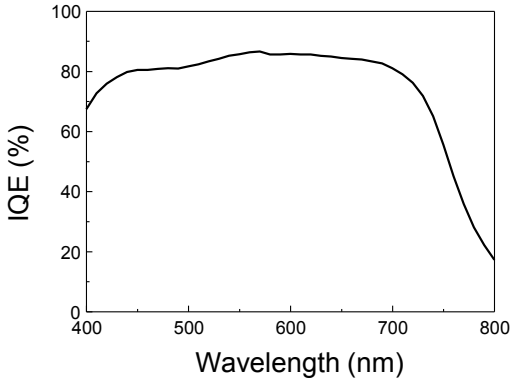

Figure S5. Internal quantum efficiency (IQE) of PTB7:PCBM calculated by division of IPCE spectrum by absorption spectrum.

Internal quantum efficiency (IQE) spectrum of PTB7:PCBM is plotted as a function of wavelength. IQE is calculated by division of IPCE spectrum by light absorption spectrum of control device. The device structure is as follows: glass substrate / ITO (150 nm) / PEDOT:PSS (40 nm) / PTB7:PCBM (80 nm) / BCP (15 nm) / Ag (120 nm).

Light absorption in top-illuminated solar cells with PEDOT:PSS (40 nm) and thin PTB7:PCBM layer (45 nm)

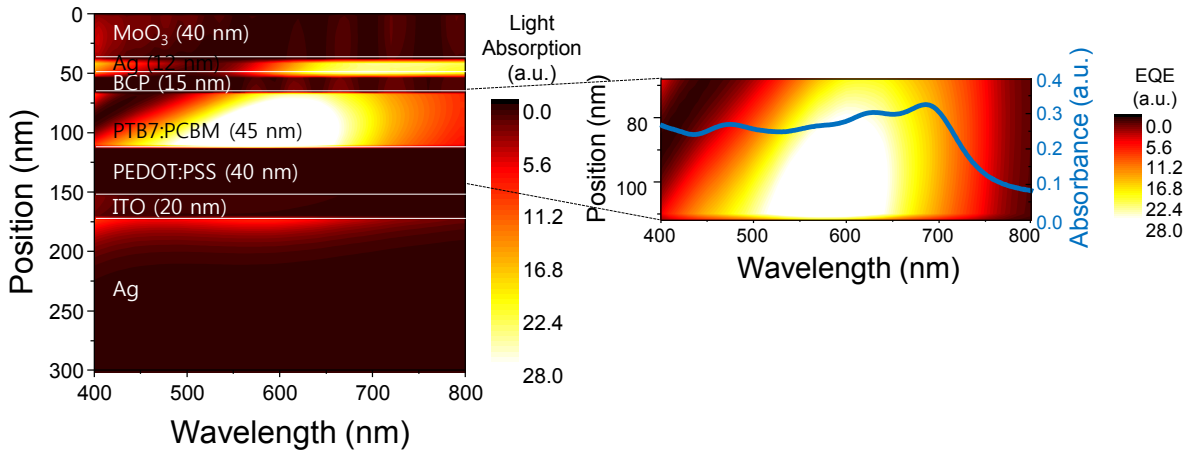

Figure S6. 2-dimensional contour of light absorption and calculated EQE in top-illuminated OSCs with PEDOT:PSS (40 nm) and thin PTB7:PCBM (45 nm) layer. Absorbance of PTB7:PCBM is plotted on the right figure.

The top-illuminated PSC with PEDOT:PSS (40 nm) and thin PTB7:PCBM (45 m) layer shows broadband light absorption on visible spectrum (λ = 500 ~ 700 nm) (Figure S6). However, the thin active layer cannot afford sufficient light absorption, thereby resulting in decreased total light absorption compared to the thick PTB7:PCBM layer (80 nm).

Flexible bottom-illuminated OSCs on PET/ITO substrate

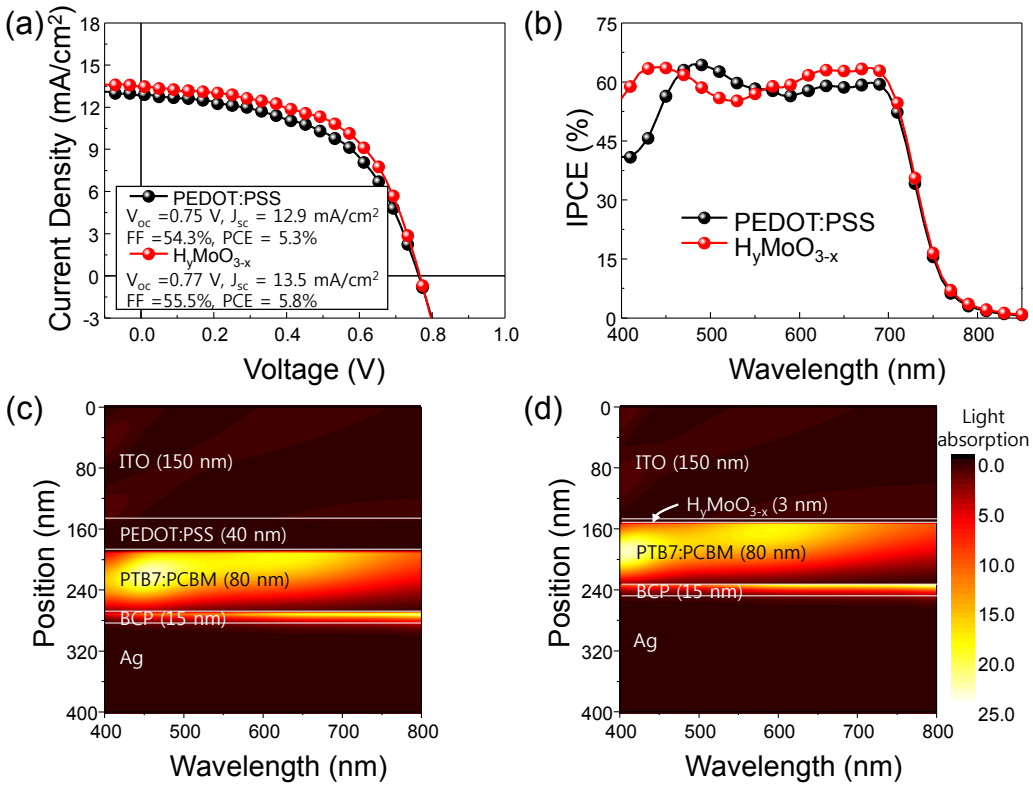

Figure S7. (a) J-V curves and (c) IPCE spectra of OSCs on PET/ITO(150 nm) substrate. The PEDOT:PSS and H_yMoO_{3-x} were used for the hole transport layer. Electric field distribution in OSCs with (a) PEDOT:PSS(40 nm) and (b) H_yMoO_{3-x} (3 nm) HTLs.

Flexible PTB7:PCBM-based organic solar cells were fabricated on PET/ITO (150 nm) substrate and J-V characteristics are indicated (Figure S7a). When the HTL is replaced from PEDOT:PSS to laser-irradiated MoO_3, the PCE enhanced from 5.3% to 5.8%. The efficiency enhancement were mainly attributed to the increased J_{sc} from 12.9 mA/cm^2 to 13.5 mA/cm^2. The OSCs with MoO_3 exhibits higher photocurrent at the short wavelength region (λ = 400 - 500 nm) than the device with PEDOT:PSS (Figure S7b). However, the IPCE spectra on visible spectrum region (λ = 400 - 800 nm) is similar to each other. The FDTD simulation shows broader band light absorption in device with MoO_3 (Figure S7c) than PEDOT:PSS (Figure S7d) because of a little enhancement of light absorption on the ultra-violet spectrum (λ = 400 - 500 nm). This result presents good agreement with measured IPCE spectra in Figure S5b.

Patterning by direct writing

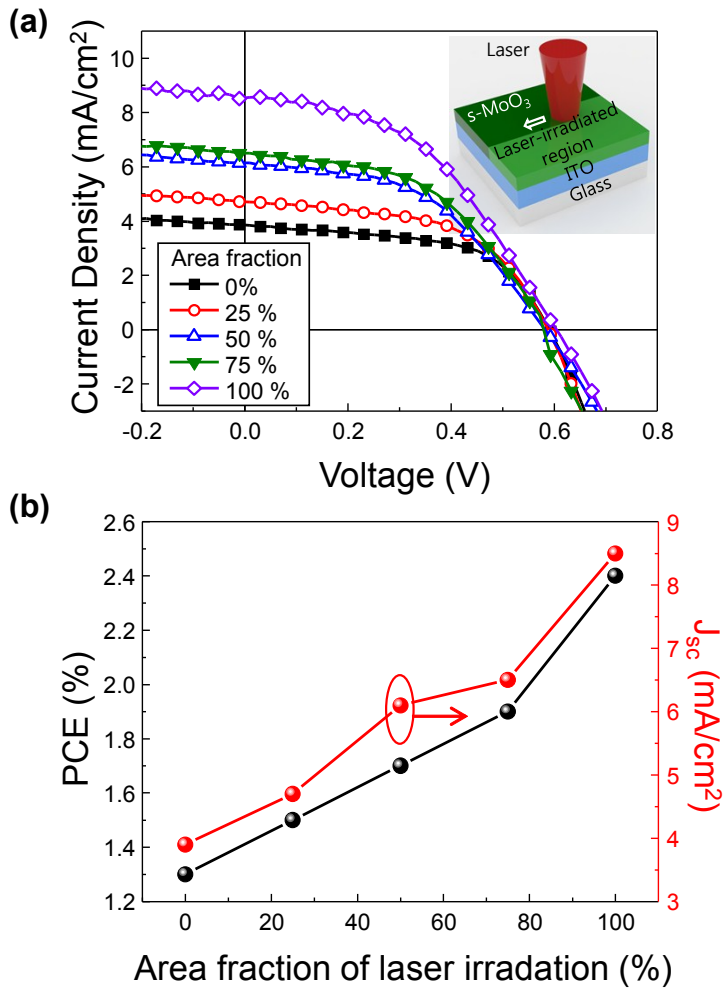

Figure S8. (a) J-V curves of P3HT:PCBM solar cells for various area fraction of laser irradiation. (b) Plot of PCE and J_{sc}.

In order to demonstrate a patterning by direct writing, P3HT:PCBM solar cells were fabricated for various area-fraction of laser irradiation. The total active area of 6.0 mm^2 was identical for all the samples. Only the area fraction of laser-irradiation was varied by 0, 25, 50, 75, and 100%. Current density increases as the larger area-fraction of laser-irradiation (Figure S8a and Table S2) due to increased electrical conductivity of laser-irradiated MoO_3 HTL. Plots of PCE and J_{sc} were indicated as a function of area-fraction of laser irradiation (Figure S8b). PCE and J_{sc} linearly correlated to the area fraction of laser-irradiation. Since the

conductivity of reduced MoO_3 is higher than that of as-coated MoO_3, the large amount of charge carriers transport through laser-irradiated MoO_3 rather than MoO_3 layer. This enhanced charge transport results in increased J_{sc}. The direct patterning and selective-area reaction can only be demonstrated by laser irradiation, cannot be achieved by thermal annealing nor UV-lamp.

Table S2. Photovoltaic characteristics of the P3HT:PCBM OSCs for different area-fraction of laser irradiation.

Area fraction of irradiation (%)	**Area w/ irradiation (cm^2)**	**Area w/o irradiation (cm^2)**	**V_{oc} (V)**	**J_{sc} (mA/cm^2)**	**FF (%)**	**PCE (%)**
0	0	0.06	0.59	3.9	57.4	1.32
25	0.015	0.045	0.59	4.7	54.0	1.50
50	0.03	0.03	0.59	6.1	49.2	1.77
75	0.045	0.015	0.59	6.5	49.9	1.91
100	0.06	0	0.59	8.4	50.2	2.48